ACS NANO
Cite This: ACS Nano 2019, 13, 5712–5719
www.acsnano.org

ARTICLE

Nanocrystal Core Size and Shape Substitutional Doping and Underlying Crystalline Order in Nanocrystal Superlattices

Davit Jishkariani,[†,∥,#] Katherine C. Elbert,[†,#] Yaoting Wu,[†,#] Jennifer D. Lee,[†] Michiel Hermes,[‡] Da Wang,[‡,⊥] Alfons van Blaaderen,[‡] and Christopher B. Murray*[,†,§]

[†]Department of Chemistry, University of Pennsylvania, Philadelphia, Pennsylvania 19104, United States
[‡]Soft Condensed Matter, Debye Institute for Nanomaterials Science, Utrecht University, Princetonplein 5, 3584 CC Utrecht, The Netherlands
[§]Department of Materials Science and Engineering, University of Pennsylvania, Philadelphia, Pennsylvania 19104, United States

Supporting Information

ABSTRACT: **Substitutional doping is a potentially powerful technique to control the properties of nanocrystal (NC) superlattices (SLs). However, not every NC can be substituted into any lattice, as the NCs have to be close in size and shape, limiting the application of substitutional doping. Here we show that this limitation can be overcome by employing ligands of various size. We show that small NCs with long ligands can be substituted into SLs of big NCs with short ligands. Furthermore, we show that shape differences can also be overcome and that cubes can substitute spheres when both are coated with long ligands. Finally, we use the NC effective ligand size, softness, and effective overall size ratio to explain observed doping behaviors.**

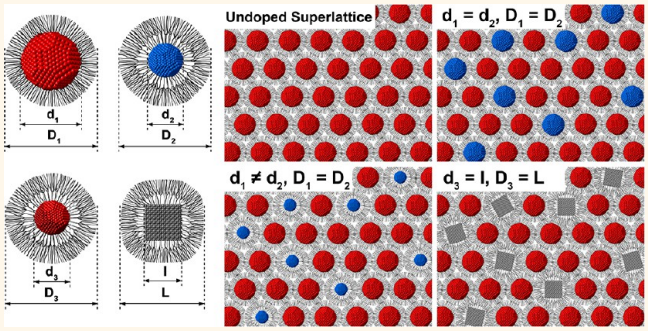

KEYWORDS: *substitutional doping, self-assembly, dendritic ligands, nanocrystal softness, nanocrystal positional preference analysis*

Metamaterials composed of two or more different building blocks can show emergent electronic,[1,2] magnetic,[3] optical,[4,5] biological,[6] and plasmonic[7] properties depending on the interactions between the components as well as the ratios between them. Doping is a process where atomic defects are intentionally introduced to a host matrix to tune its properties.[8,9] Substitutional doping in colloid science is a mesoscale approach where uniform nanocrystals (NCs) are introduced into ordered superlattices (SLs) composed of different NCs, where they occupy random positions without sacrificing the overall film crystallinity.[10] As opposed to atomic size impurities, the size and the shape of NC building blocks can be tuned. The doping process is known to require uniform NCs that have similar size and shape, as typically NCs of differing morphology self-segregate.[11] Generally, during the NC self-assembly process where the inorganic core is larger than 3 nm, the main considerations are the dimensions of the inorganic core. This is due to the fact that in the vast majority of NC systems, the core dimensions are far larger than the ligand dimensions, and therefore the size of ligand is neglected. Also, in most cases, the nature and the size of the ligands are similar, as only a few commercial ligands (oleic acid, oleylamine, trioctylphosphine, *etc.*) are generally used to synthesize the vast majority of colloidal NCs.[12−15] However, engineering the nature and size of the organic ligands present on NC surfaces allows a more precise control of the NC assembly process,[16−18] particularly in applications such as altering or introducing optical,[19,20] electronic,[21,22] magnetic,[23,24] catalytic,[25,26] enhanced colloidal stability/dispersibility,[27] and self-assembly properties.[28] Recently, monodisperse bulky ligands such as dendritic macromolecules[19,29] have attracted considerable interest due to their highly flexible synthesis where the size, surface binding ability, and the nature of the end-groups can be independently altered to create a custom ligand with desired properties. When large dendrimers are attached to small NCs, they can increase the effective size of the NC such that the self-assembly behavior can no longer be predicted by inorganic core sizes only.[19,28]

In substitutional doping, successful doping depends on the size and the shape similarity of the NCs, where avoiding a mismatch between the physical dimensions enables the SL to

Received: February 8, 2019
Accepted: May 3, 2019
Published: May 3, 2019

DOI: 10.1021/acsnano.9b01107
ACS Nano 2019, 13, 5712–5719

accommodate the dopant NCs. To overcome these limitations, we explore the role of ligands by introducing different sized bulky dendritic ligands on NC surfaces, where NC-dendrimer hybrids have a larger overall size (core + ligand), thus the overall size of the hybrids must be considered as opposed to just the inorganic core.

Surface coating with a dendritic ligand would create a large organic coating that introduces softness and could mask the physical properties such as the size and shape of the NCs in dried films similar to the use of surface charge and a solvent with long screening length.[30] For simplicity, the softness is quantified as the effective length of the ligand divided by the sum of the effective ligand length and NC core radius, and the values are expressed in (%) by multiplying them by 100 (Table S1). The effective ligand length itself is derived from transmission electron microscopy (TEM) images of corresponding single component self-assembled SLs by dividing the NC edge-to-edge distance by two (Table S1).

These hybrids can be used to dope a NC SL with NCs of differing size or shape, as the ligands on the NC surfaces create hybrids of similar dimensions. By doing so, the NC size and shape can be masked, and as a result, the NC size and shape and SL architecture can be decoupled from one another. Here we demonstrate the use of bulky ligands to overcome the NC size and shape difference, achieving NC core size and shape substitutional doping. Large, monodisperse dendritic ligands can enable this phenomenon, as they introduce thick organic shells on NC surfaces and increase the overall size of hybrids (Figure 1). Therefore, it is possible to dope a SL of larger inorganic core NCs coated with a smaller organic shell with smaller NCs coated with a larger organic ligand, and *vice versa*, demonstrating that the NC core size similarity is no longer a strict requirement. Interestingly, what appears to be a random doping at low dopant concentration (<10%) reveals an underlying order at higher dopant concentrations (>10%), where the positions of dopant and host NCs display positional preference while still maintaining excellent overall SL ordering. Such structures are identical to single component SLs in terms of overall film crystallinity. However, an intermediate state appears between the binary and the single component SLs, characterized by individual NC positional order. These structural features are observed both with same and different sized NCs assemblies. The use of large ligands was found to overcome the shape difference of NCs as well. The mix of similarly sized spherical and cubic NCs, once they are coated with dendritic ligands, can co-assemble into crystalline SLs, avoiding the need of inorganic core shape similarity.

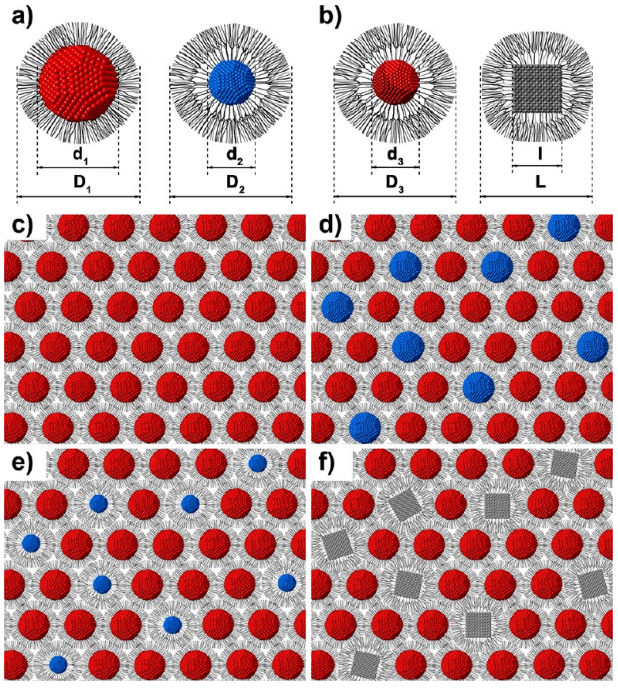

Figure 1. Schematic representation of the inorganic core and whole NC dimensions for different sized (a) spherical NCs and (b) spherical and cubic NCs where a similar overall size can be achieved using bulky ligands as well as schematic representation of self-assembled monolayers of (c) single component SL, (d) substitutional doping, (e) size substitutional doping, and (f) shape substitutional doping in NC SLs.

RESULTS AND DISCUSSION

To explore the NC doping concept further, we first chose three different sizes of oleylamine-coated Au NCs: 5.2 ± 0.5 nm, 7.6 ± 0.5 nm, and 10.2 ± 0.6 nm (Table S1). When considered separately, they form ordered single component SLs, but do not form substitutionally doped films upon mixing, as highlighted in Figure S1 and Table S1, entries 1−6. To increase the stability of Au NCs during the self-assembly process and avoid ligand related unfavorable interaction, the native ligand oleylamine was replaced with the small and the large dendrimers **1** and **2** (Figure 2) that have identical surface binding disulfide and terminal dodecyl groups but are different in their size due to a different number of branches.[31]

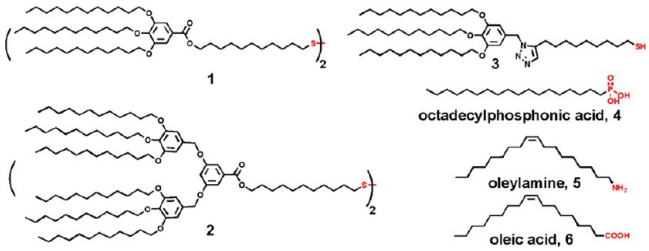

Figure 2. Structures of dendritic 1−3 and alkyl chain ligands 4−6.

As a preliminary study, self-assembly of six sample combinations were studied by the well-developed liquid−air interface method using diethylene glycol as a subphase.[32] First, TEM analysis of self-assembled monolayers from single component NC solutions (Figure S1) gave information about the size of the inorganic core and an effective length of each ligand (interparticle separation divided by two) on different sized NCs.[31] This information was used to deduce the overall effective size of each NC-dendrimer hybrid. Second, self-assembly of binary mixtures were systematically evaluated, using the library of different sized NCs coated with either small dendrimer **1** or large dendrimer **2**. We targeted the self-assembled monolayer due to its simplicity compared to multilayers and studied the possibility of all four major self-assembly motifs: substitutional doping, phase separation, mixed but disordered phases, and binary nanocrystal SLs (BNSLs). Depending on the mixing pair, the emerging motifs were identified (Table S2).

Successful NC substitutional doping was observed when 5.2 ± 0.5 nm Au NCs coated with large dendrimer **2** (denoted

DOI: 10.1021/acsnano.9b01107
ACS Nano 2019, 13, 5712−5719

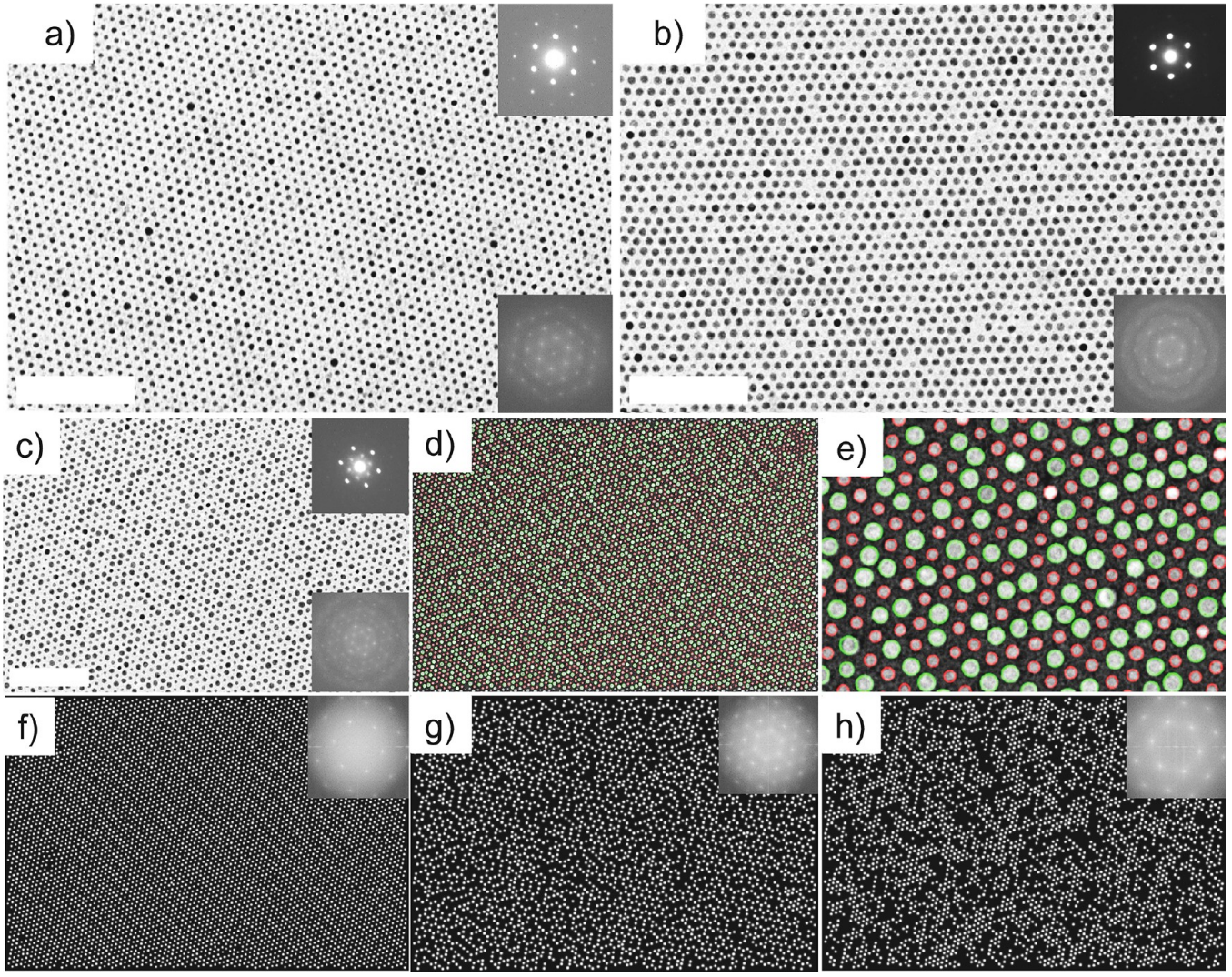

Figure 3. TEM micrographs of self-assembled structures obtained from binary mixtures of 5.2 ± 0.5 nm Au@2 and 7.6 ± 0.5 nm Au@1 (a) 9:1 ratio, (b) 1:9 ratio, (c) 1:1 ratio. Scale bars are 100 nm, upper and lower right insets are SAED and FFT patterns, respectively. (d) Particle tracking from (c), where 5.2 nm Au@2 are falsely colored red and 7.6 nm Au@1 are falsely colored green, (e) higher magnification of (d), (f) all of the NCs drawn at the same size, (g) image (f) with only the 5.2 ± 0.5 nm NCs, and (h) a randomly chosen fraction of the particles in (f). Upper right insets in (e, g, and h) are FFT patterns.

Au@**2**) were mixed with 7.6 ± 0.5 nm Au@**1**, as shown in Figure 3a–c. Excellent doping was obtained for tested ratios of 9:1, 1:9, and 1:1, where the crystallinity of the SL is maintained, as highlighted by the associated small-angle selected area electron diffraction (SAED) and fast Fourier transform (FFT) patterns. Substitutional doping is observed for the closest size of the hybrid taking the core and the ligand layer into account, that is, 10.6 and 11.1 nm, corresponding to a maximized whole particle diameter ratio of 0.96 (Table S2). The order of substitution was analyzed in the sample with a 1:1 ratio by particle tracking analysis, an example of which is fully described in Figure S3, comparing the number of neighbors of both species, as shown in Figures 3d–h and S4.[33] To track the NCs, each NC was initially made to be the same size, highlighted by Figure 3d,e, where the small NCs are falsely colored red and the large NCs are falsely colored green. When the NCs are adjusted to be equivalent sizes, the SL that they form is shown in Figure 3f. The small NCs have 3.0 large neighbors on average, while the large NCs only have 1.3 large neighbors (Figure S4). Such a difference is indicative of a nonrandom distribution with a preference for small-to-large NC pairing, which is highlighted by Figure 3g, where a hexagonal honeycomb pattern is apparent once the large NCs are removed from the SL. Comparing the SL positions of the small NCs in Figure 3g to the pattern of a random distribution of positions in the equivalent lattice in Figure 3h, it is clear that this doping is not random.

Bilayer films of this example maintain this doping phenomenon, as shown in Figure 4a. Substitutional doping was also observed when 7.6 ± 0.5 nm Au@**2** was mixed with 10.2 ± 0.6 nm Au@**1** (Figure 4b), with overall sizes of 13.2 and 12.7 nm, respectively. However, despite the very similar overall effective size (whole particle diameter ratio of 0.96), disordered phases and self-separation motifs were also observed (Figure 4c, Table S2). This is most likely due to the ability of the larger dendritic ligand **2** to overcome NC–NC interactions compared to the smaller ligand **1**. As shown previously, as the NC size increases, larger ligands are effective at maintaining interparticle spacing.[31] This can be quantified by NC softness (%), defined as the length of the ligand divided

DOI: 10.1021/acsnano.9b01107
ACS Nano 2019, 13, 5712–5719

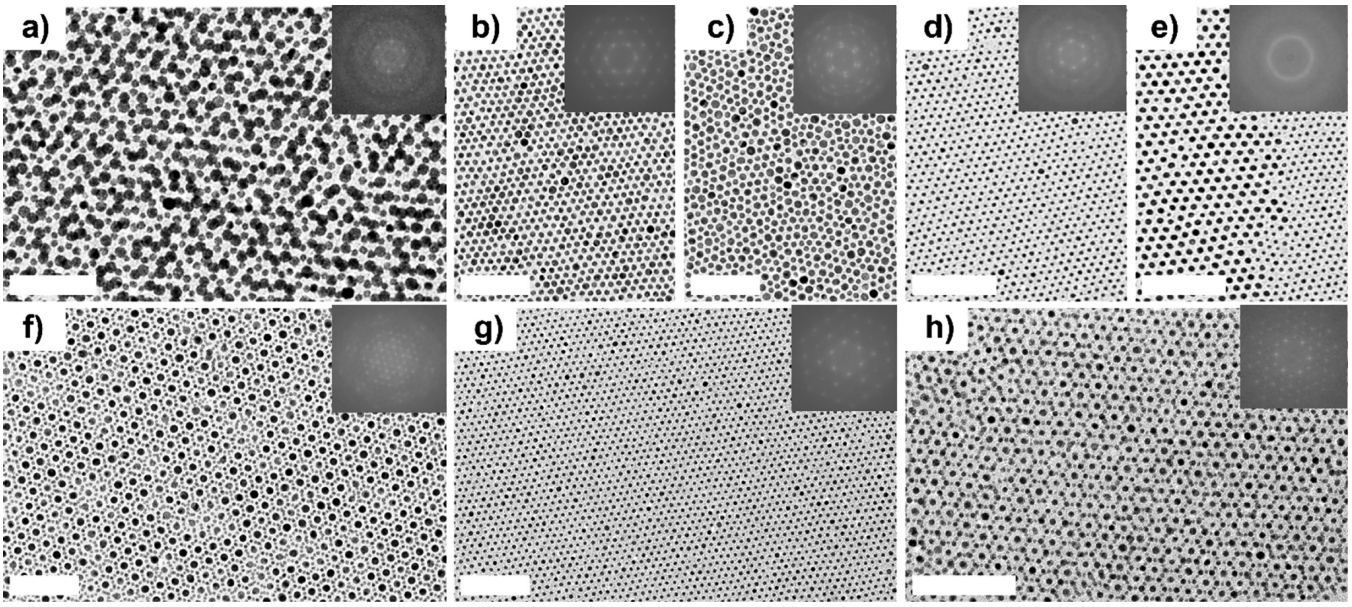

Figure 4. TEM micrographs of (a) bilayer of 5.2 ± 0.5 nm Au@2 and 7.6 ± 0.5 nm Au@1, (b) and (c) 5.2 ± 0.5 nm Au@2 and 7.6 ± 0.5 nm Au@2, (d) and (e) 7.6 ± 0.5 nm Au@2 and 10.2 ± 0.6 nm Au@1, (f) 5.2 ± 0.5 nm Au@2 and 10.2 ± 0.6 nm Au@2, and (g) and (h) 5.2 ± 0.5 nm Au@2 and 6.1 ± 0.5 nm Au@1. Scale bar in (a) is 50 nm, and in (b–h) 100 nm. FFT patterns of every image are shown in the insets.

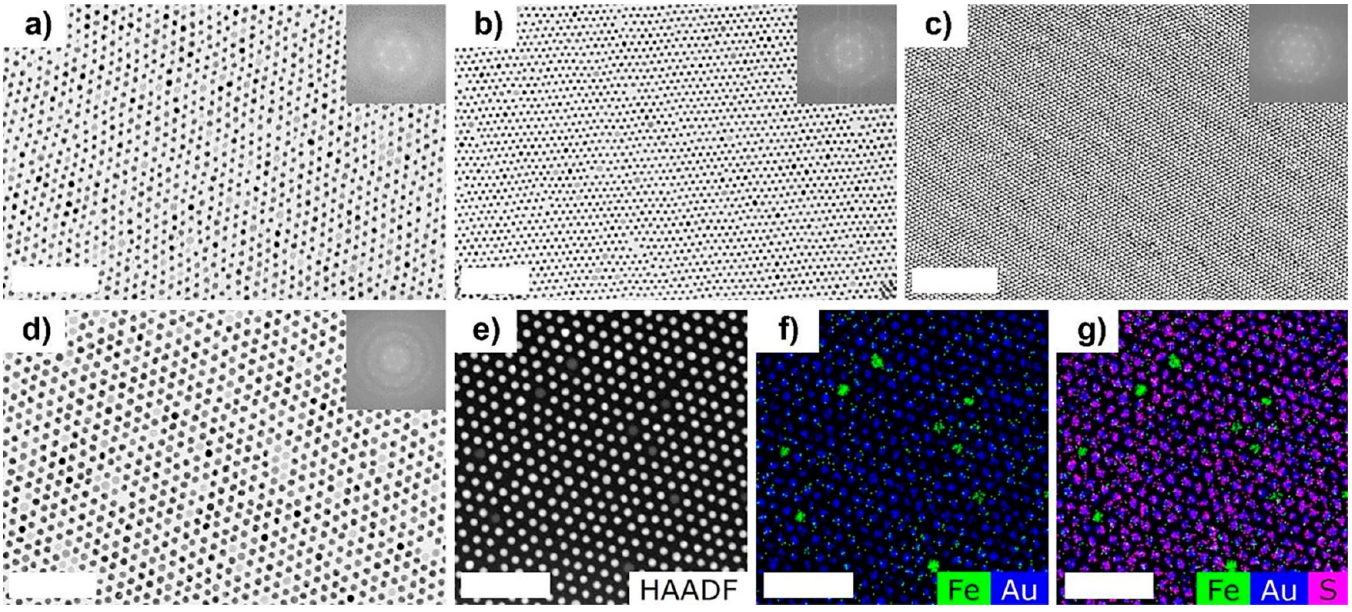

Figure 5. TEM micrographs of size or shape substitutional doping structures obtained from binary mixtures of (a) 7.6 ± 0.5 nm Au@2 and 9.5 ± 0.8 nm $Mn_{0.08}Zn_{0.33}Fe_{2.59}O_4$@4, (b) and (c) 6.6 ± 0.4 nm Au@2 and 8.9 ± 0.8 nm $Mn_{0.08}Zn_{0.33}Fe_{2.59}O_4$@4, (d) 10.2 ± 0.6 nm Au@2 and 9.5 ± 0.8 nm $Mn_{0.08}Zn_{0.33}Fe_{2.59}O_4$@4, and (e–g) EDX chemical mapping of doped SLs obtained with 6.6 ± 0.4 nm Au@2 and 8.9 ± 0.8 nm $Mn_{0.08}Zn_{0.33}Fe_{2.59}O_4$. Scale bars in (a, b, d–h) are 100 nm, in (c) 200 nm, and in (e–g) 50 nm. FFT patterns for (a–d) are shown in the insets.

by the sum of the ligand length and NC core radius and the value expressed as (%) by multiplying by 100 (Table S1). For 7.6 ± 0.5 nm Au@**2** and 10.2 ± 0.6 nm Au@**1**, the NC softness is 42.4% and 19.7%, respectively, as shown in Table S1. With a significantly smaller softness, 10.2 ± 0.6 nm Au@**1** is less likely to accommodate the size mismatch in the SL than 7.6 ± 0.5 nm Au@**2**, giving rise to self-separation motifs in the film. By comparison, successful doping throughout the film is observed from a mixture of 5.2 ± 0.5 nm Au@**2** and 7.6 ± 0.5 nm Au@**1**, with a NC softness of 50.9% and 31.5%, respectively. An additional NC size of 6.1 ± 0.5 nm was coated with **1** and mixed with 7.6 ± 0.5 nm Au@**2** to confirm that both NC softness and whole particle sizes are key components to successfully doping a SL. As shown in Figure 4g, substitutional doping is also observed in this SL, which is consistent with previous examples as the NC softness of these particles is 39.2% and 42.4%, respectively, and the whole particle size ratio is 0.95 (Tables S1 and S2). This highlights that both high NC softness and whole particle sizes are essential parameters toward a successful substitutional doping.

This finding is supported by the fact that doping can also be observed in a mixture comprising 5.2 ± 0.5 and 7.6 ± 0.5 nm

DOI: 10.1021/acsnano.9b01107
ACS Nano 2019, 13, 5712–5719

NCs both coated with larger dendrimer **2**, as shown in Figure 4d. However, this sample showed only a moderate doping and mostly consisted of the self-separated domains (Figure 4e). The whole particle diameter ratio of 0.80 is significantly smaller, demonstrating the required balance that has to be found in between NC softness and whole size matching, in order to yield SL formation along the whole film. Other binary mixtures have revealed either self-separation between smaller and larger NCs domains, such as in Figure S4a, mixed but disordered layers (Table S2, Figures 4c and S4b), or in some cases, when the NC overall effective sizes and their local concentration were suitable, more complex binary SL domains that are isostructural to $CaCu_5$ were formed (Figures 4f,h and S4d and S5).

Interestingly, doping, binary SLs, or even mixed, but disordered phases were predominantly observed in the mixtures where at least one NC sample was coated with larger dendrimer **2**. In mixtures where both NC samples were coated with smaller dendrimer **1**, only self-separation occurs. This observation bolsters the importance of a thick monodisperse organic shell which can overcome the size irregularity during the self-assembly and improve the quality of the film crystallinity.[34,35]

For the systems studied in this work, successful doping is observed only when the host NCs have a softness of higher or equal to 31.5% (Table S1) as well as an effective whole particle diameter ratio of at least 0.78 (Table S2). For cases where the whole particle diameter ratio was >0.78, but the NC softness of the host lattice was <31.5%, self-separation was observed. Similarly, doping was not detected in mixtures where the softness is >31.5%, but effective overall diameter ratio is <0.78 (Table S2). This leads us to believe that to predict successful substitutional doping with NCs of differing inorganic core sizes, both factors need to be taken into account.

To further explore the possible guidelines for substitutional doping, investigations into using NCs with different inorganic materials as well as NCs with different shapes were conducted. Experiments using NCs made with different inorganic materials and coated with octadecylphosphonic acid **4** showed that substitutional doping takes place even when the ligand architecture is different, as long as the end-group of the ligands is similar in nature. For example, the doping of large dendron **2** coated 6.6 ± 0.4 nm Au NC SL with 8.9 ± 0.8 nm manganese zinc ferrite, $Mn_{0.08}Zn_{0.33}Fe_{2.59}O_4$ NCs was successful (Figure 5b,c) only when the native ligand, oleic acid **6**, was replaced with octadecylphosphonic acid **4**. When the oleic acid coated $Mn_{0.08}Zn_{0.33}Fe_{2.59}O_4$ NCs were mixed with dendron coated NCs, negligible doping and mostly a self-separation was observed (Figure S7), revealing that the nature of the ligand end groups may also have an influence on doping and the difference between end-groups might cause NC self-segregation. However, more research is needed to explore the role of ligand end-groups and its influence on NC mixing energy.

Figure 5 shows the TEM images of SLs obtained from the combination of octadecylphosphonic acid **4** coated 9.5 ± 0.8 nm $Mn_{0.08}Zn_{0.33}Fe_{2.59}O_4$ and large dendron **2** coated 7.6 ± 0.5 nm Au as well as single (Figure 5b) and multilayer (Figure 5c) SLs of ligand **4** coated 8.9 ± 0.8 nm $Mn_{0.08}Zn_{0.33}Fe_{2.59}O_4$ doped 6.6 ± 0.4 nm Au. The successful substitutional doping in the latter example was studied by energy dispersive X-ray spectroscopy (EDX) mapping shown in Figures 5e–g and S8. The results confirm the presence of both NC types in the SLs as well as the presence of the sulfide-based ligand **2** on the Au NCs. Figure 5d represents a control example obtained by mixing relatively similarly sized inorganic NCs coated with different sized ligands. 10.2 ± 0.5 nm Au@**2** is mixed with ligand **4** coated 9.5 ± 0.8 nm $Mn_{0.08}Zn_{0.33}Fe_{2.59}O_4$ NCs. Regardless of the large difference in ligand size, the assembly maintains large-scale ordering, as also seen in Figures 5d and S9. Such a result is explained by the presence of large, yet flexible ligands on the Au NC surfaces that produce softer NCs (33.8%), causing a decrease of the lattice strain while maintaining the overall NC size ratio of 0.84. However, the tendency toward the clustering of $Mn_{0.08}Zn_{0.33}Fe_{2.59}O_4$ NCs is also obvious (Figures 5d and S9). In these SLs, a large portion of NCs seems to group into small clusters (>3 NCs side by side), a phenomenon that may be explained by the combination of factors such as a difference in ligand size and the magnetic dipole–dipole interaction between $Mn_{0.08}Zn_{0.33}Fe_{2.59}O_4$ NCs.

To study the effect of NC shape, experiments using 9.5 ± 0.8 nm (side) cubic Pt NCs as building blocks to dope spherical NC SLs revealed substitutional doping that is independent of the shape of the components, where the cubic NCs occupy random positions in close packed hexagonal SLs. Figures 6a, 7a, and S11 show close packed single layer SLs

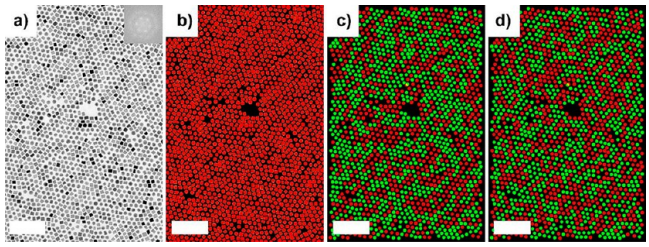

Figure 6. (a) TEM micrograph of a doped SL obtained from 10.2 ± 0.6 nm Au@3 and 9.5 ± 0.8 nm Pt cubes@3 and (b) its particle tracking analysis where all particles are falsely colored red. (c) All particles as spheres, where Pt cube positions are represented with green spheres and Au sphere positions are represented with red spheres. (d) A software generated example for a random arrangement within the SL. Scale bars are 100 nm, and FFT pattern is shown in (a) as an inset.

where lattice sites are randomly occupied by either smaller dendron **3** (Figures 6a and S11) or larger dendron **2** coated (Figure 7a) spherical 10.2 ± 0.6 nm Au and smaller dendron **3** coated 9.5 ± 0.8 nm (side) cubic Pt NCs.

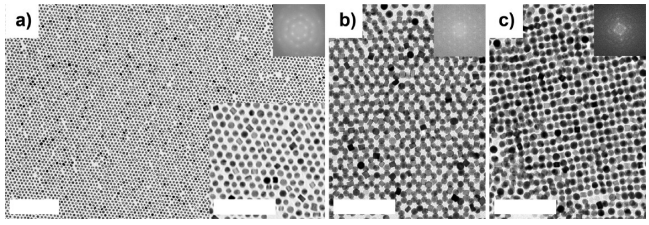

Figure 7. Structural diversity in doped SLs obtained from the mixture of 10.2 ± 0.6 nmAu@2 and 9.5 ± 0.8 nm Pt cubes@3. TEM micrographs of low- (a) and high-resolution (inset in a) close-packed single layer, close packed bilayer (b), and AB-type binary (c) SLs are shown. FFTs are provided as insets. Scale bars are 100 nm.

DOI: 10.1021/acsnano.9b01107
ACS Nano 2019, 13, 5712–5719

Particle tracking analysis (Figure 6b–d) of the doped SL shown in Figure 6a reveals that the cubes have on average 2.3 cubes as neighbors and the spheres have on average 2.6 cubes as neighbors, as shown in Figure S12. This small difference indicates a very small or negligible positional preference. Thus, the positions of cubic NCs within the SLs are very close to random, indicating almost complete masking of the differences in the interactions between the different NCs.

Interestingly, when 10.2 ± 0.6 nm Au@**2** NC is mixed with 9.5 ± 0.8 nm Pt cubes@**3**, the observed doped SLs reveal two distinctly different self-assembled motifs: hexagonal-close packed doped single (Figure 7a)[36] and bilayers (Figure 7b), as well as cubic AB type binary structures shown in Figure 7c. Successful doping is observed in all of those domains. Compared to the smaller dendron coated Au NC systems (Figures 6a and S10a,b), the use of larger dendron **2** coated Au NCs (Figure 7a–c) seems to improve the overall film crystallinity. This can be again attributed to the NC softness factor, which is 51.0% for Au@**2** and 27.5% for Au@**3** when the Au NCs are 10.2 ± 0.6 nm. When hosting 9.5 ± 0.8 nm Pt cubes@**3**, the larger ligand can mask the NC shape and accommodate cubic NCs more effectively than a ligand of similar architecture but smaller size. The presence of different self-assembly motifs within the same sample is probably due to the confinement effect caused by a film thickness.[37]

CONCLUSIONS

In conclusion, we report that substitutional doping can be achieved with different sized or shaped inorganic NCs when the surfaces are modified using ligands that are large enough to be able to mask the size and shape differences as well as match the overall effective size and the shape of the NCs. Experiments reveal the trend that ligands with longer effective length, also described as having high softness, minimize the self-separation and increase the chance of successful doping, to a certain extent. Furthermore, the experiments have shown that at high dopant concentrations, the substitution is not always fully random but that different amounts of order are possible, offering an additional route to control the microstructure. Further research is needed to elucidate other possible factors that may contribute to enabling or hindering the formation of substitutionally doped two-dimensional (2D) and three-dimensional structures. We expect this technique to show promise in many areas, as its versatility offers the opportunity to combine properties of multiple NCs into metamaterials.

METHODS

Materials. 1-Octadecene (technical grade, 90%), manganese(II) acetylacetonate, zinc(II) acetylacetonate (≥98%), and iron(III) acetylacetonate (99+%) was purchased from Acros Organics. Trioctylphosphine (97%), benzyl ether (98%), oleic acid (technical grade, 90%), and oleylamine (technical grade, 70%) were purchased from Sigma-Aldrich. All of the chemicals were used as received. Solvents were ACS grade or higher.

Synthesis of Au NCs. Au NCs used in this study were synthesized following reported procedures.[31] To synthesize the 5.2 nm Au NCs, 200 mg of $HAuCl_4 \cdot 3H_2O$ was dissolved in 10 mL of tetralin and 10 mL of oleylamine (Olam) under a flow nitrogen with magnetic stirring. Then, a mixture containing 90 mg of borane *tert*-butylamine (TBAB) dissolved in 1 mL of tetralin and 1 mL of oleylamine was injected into the $HAuCl_4$ solution. The solution turned deep red immediately, and the reaction was kept at room temperature for 2 h. Then, acetone (120 mL) was added to the reaction, and the mixture was centrifuged at 8000 rpm for 3 min. The collected Au NCs were redispersed in 20 mL of hexane, precipitated twice more by using 120 mL of ethanol, and centrifuged at 8000 rpm for 3 min. The particles were stored in hexane for further use.

To synthesize the 7.6 nm Au NCs, 100 mg $HAuCl_4 \cdot 3H_2O$ was dissolved in 20 mL of octadecene and 1 mL of Olam under a flow of nitrogen with magnetic stirring. Then, 30 mg of the 5.2 nm Au NCs suspended in hexane were injected into the solution as seeds for growth. The mixture was kept at 60 °C for 2 h, and then purified three times by adding 120 mL of ethanol and centrifuging at 8000 rpm for 2 min after the reaction cools to room temperature. The washed Au NCs were stored in hexane for further use. The synthesis of the 10.2 nm Au NCs followed the same recipe as described above but used 7.6 nm Au NPs as seeds instead.

Synthesis of Pt Cubes. Pt nanocubes were prepared according to the literature procedure.[38]

Synthesis of $Mn_{0.08}Zn_{0.33}Fe_{2.59}O_4$ (MZF) NCs. MZF NCs used in this study were synthesized following reported procedures.[23] Mn (II) acetylacetonate (3 mmol), zinc(II) acetylacetonate (6 mmol), iron(III) acetylacetonate (12 mmol), oleic acid (100 mmol), oleylamine (112 mmol), and 1-octadecene (72 mL) were mixed in a 250 mL flask. The reaction mixture was heated to 110 °C and kept under vacuum for 2 h. Then, the temperature was increased to 300 °C at a rate of 11 °C/min. After 2 h, the reaction mixture is cooled down to the room temperature, and zinc ferrite NCs are precipitated by adding isopropanol. Manganese zinc ferrite NCs were redispersed in hexane and washed further using isopropanol three times. The ratio between zinc and iron is measured by inductive coupling plasma-optical emission spectrometry (ICP-OES) performed on a Spectro Genesis spectrometer with a concentric nebulizer.

Ligand Exchange on MZF NCs with Octadecane Phosphonic Acid. To a stirred solution of MZF NCs (10 mg) in chloroform (10 mL) was added octadecane phosphonic acid (10 mg), and the resulting solution was stirred overnight at 35 °C. MZF NCs were precipitated out of solution using methanol (30 mL). After centrifugation, the NCs were redispersed in chloroform. This procedure was repeated 2–3 times to ensure the complete removal of any unbound or replaced ligand.

Ligand Exchange on Au and Pt NCs with Dendrons. Ligand exchange on the oleic acid capped metal (Pt, Au) NCs was performed by mixing 1 mL of NCs (10 mg/mL) in hexanes with the 1 mL chloroform solution (10 mg/mL) of dendritic ligand. To ensure the complete exchange, the resulting solution was stirred for 2 h (overnight at 35 °C, for Pt NCs). The reaction was stopped by precipitation of the NCs with excess methanol, and the NCs were collected by centrifugation. The solid (NCs) was collected and redispersed in chloroform. This procedure was repeated 3 times to ensure the complete removal of any unbound organic molecules.

Self-Assembly of NCs. NC self-assembly was performed on liquid–air interface using previously described methods.[31,32] A few drops of dendronized NCs in hexanes (concentration 5–10 mg/mL) was cast onto a diethylene glycol surface placed into 1.5 $cm^2 \times 1.0$ cm deep Teflon well. The system was covered immediately with a glass (microscope slide) to slow the solvent evaporation and left until hexane layer evaporated. Once the hexane evaporated, the floating NC film was transferred onto TEM grids by scooping up sections of it from below. Residual diethylene glycol was removed from TEM grid by placing it in a high-vacuum chamber before imaging by TEM.

Electron Microscopy. TEM micrographs were collected using a JEOL 1400 microscope operated at 120 kV. The TEM was calibrated using a MAG*I*CAL TEM calibration standard.

2D EDX Chemical Mapping Measurements. 2D EDX chemical mapping measurements were performed using a FEI Talos F200X transmission electron microscope, equipped with a high-brightness field emission gun (X-FEG) and a Super-X G2 EDX detector operated at 200 kV. Images and elemental EDX maps were acquired using Bruker Esprit analytical and imaging software in scanning transmission mode. Elemental EDX maps of 802 × 801 pixels were acquired with a 15 min acquisition time to get a good signal-to-noise ratio.

DOI: 10.1021/acsnano.9b01107
ACS Nano 2019, 13, 5712–5719

ASSOCIATED CONTENT

Supporting Information

The Supporting Information is available free of charge on the ACS Publications website at DOI: 10.1021/acsnano.9b01107.

Synthesis procedures, additional microscopy and data analysis (PDF)

AUTHOR INFORMATION

Corresponding Author

*E-mail: cbmurray@sas.upenn.edu.

ORCID

Davit Jishkariani: 0000-0003-3771-2645

Katherine C. Elbert: 0000-0001-9019-1506

Yaoting Wu: 0000-0002-4363-9870

Jennifer D. Lee: 0000-0003-2644-3507

Present Addresses

[‖]Chemical and Nanoparticle Synthesis Core (CNSC), University of Pennsylvania, Philadelphia, PA 19104, United States

[⊥]Electron Microscopy for Materials Science (EMAT), University of Antwerp, Groenenborgerlaan 171, 2020 Antwerp, Belgium

Author Contributions

[#]These authors contributed equally.

Notes

The authors declare the following competing financial interest(s): Aspects of this work have been included in a U.S. provisional patent filing.

ACKNOWLEDGMENTS

This work was supported by the University of Pennsylvania's NSF MRSEC under award no. DMR-112090 and the CNRS-UPENN-SOLVAY through the Complex Assemblies of Soft Matter Laboratory (COMPASS). K.C.E. acknowledges support from the NSF Graduate Research Fellowship Program under grant no. DGE-1321851. C.B.M. acknowledges the Richard Perry University Professorship at the University of Pennsylvania. D.W. and A.v.B. acknowledge partial funding from the European Research Council under the European Union's Seventh Framework Programme (FP-2007-2013)/ERC Advanced Grant Agreement 291667 HierarSACol. M.H. was supported by The Netherlands Center for Multiscale Catalytic Energy Conversion (MCEC), an NWO Gravitation programme funded by the Ministry of Education, Culture and Science of the government of The Netherlands. The authors thank EM square in Utrecht University for the access to the microscopes.

REFERENCES

(1) Urban, J. J.; Talapin, D. V.; Shevchenko, E. V.; Kagan, C. R.; Murray, C. B. Synergism in Binary Nanocrystal Superlattices Leads to Enhanced *P*-Type Conductivity in Self-Assembled PbTe/Ag2Te Thin Films. *Nat. Mater.* **2007**, *6*, 115−121.

(2) Shevchenko, E. V.; Talapin, D. V.; Kotov, N. a; O'Brien, S.; Murray, C. B. Structural Diversity in Binary Nanoparticle Superlattices. *Nature* **2006**, *439*, 55−59.

(3) Chen, J.; Dong, A.; Cai, J.; Ye, X.; Kang, Y.; Kikkawa, J. M.; Murray, C. B. Collective Dipolar Interactions in Self-Assembled Magnetic Binary Nanocrystal Superlattice Membranes. *Nano Lett.* **2010**, *10*, 5103−5108.

(4) O'Brien, E. S.; Trinh, M. T.; Kann, R. L.; Chen, J.; Elbaz, G. A.; Masurkar, A.; Atallah, T. L.; Paley, M. V.; Patel, N.; Paley, D. W.; Kymissis, I.; Crowther, A. C.; Millis, A. J.; Reichman, D. R.; Zhu, X.-Y.; Roy, X. Single-Crystal-to-Single-Crystal Intercalation of a Low-Bandgap Superatomic Crystal. *Nat. Chem.* **2017**, *9*, 1170−1174.

(5) Zhang, Y.; Lu, F.; Yager, K. G.; van der Lelie, D.; Gang, O. A General Strategy for the DNA-Mediated Self-Assembly of Functional Nanoparticles into Heterogeneous Systems. *Nat. Nanotechnol.* **2013**, *8*, 865−872.

(6) Nykypanchuk, D.; Maye, M. M.; van der Lelie, D.; Gang, O. DNA-Guided Crystallization of Colloidal Nanoparticles. *Nature* **2008**, *451*, 549−552.

(7) Myers, B. D.; Lin, Q.-Y.; Wu, H.; Luijten, E.; Mirkin, C. A.; Dravid, V. P. Size-Selective Nanoparticle Assembly on Substrates by DNA Density Patterning. *ACS Nano* **2016**, *10*, 5679−5686.

(8) Erwin, S. C.; Zu, L.; Haftel, M. I.; Efros, A. L.; Kennedy, T. A.; Norris, D. J. Doping Semiconductor Nanocrystals. *Nature* **2005**, *436*, 91−94.

(9) Umebayashi, T.; Yamaki, T.; Itoh, H.; Asai, K. Band Gap Narrowing of Titanium Dioxide by Sulfur Doping. *Appl. Phys. Lett.* **2002**, *81*, 454−456.

(10) Cargnello, M.; Johnston-Peck, A. C.; Diroll, B. T.; Wong, E.; Datta, B.; Damodhar, D.; Doan-Nguyen, V. V. T.; Herzing, A. A.; Kagan, C. R.; Murray, C. B. Substitutional Doping in Nanocrystal Superlattices. *Nature* **2015**, *524*, 450−453.

(11) Bishop, K. J. M.; Wilmer, C. E.; Soh, S.; Grzybowski, B. A. Nanoscale Forces and Their Uses in Self-Assembly. *Small* **2009**, *5*, 1600−1630.

(12) Grzelczak, M.; Pérez-Juste, J.; Mulvaney, P.; Liz-Marzán, L. M. Shape Control in Gold Nanoparticle Synthesis. *Chem. Soc. Rev.* **2008**, *37*, 1783−1791.

(13) Astruc, D.; Boisselier, E.; Ornelas, C. Dendrimers Designed for Functions: From Physical, Photophysical, and Supramolecular Properties to Applications in Sensing, Catalysis, Molecular Electronics, Photonics, and Nanomedicine. *Chem. Rev.* **2010**, *110*, 1857−1959.

(14) Daniel, M.-C.; Astruc, D. Gold Nanoparticles: Assembly, Supramolecular Chemistry, Quantum-Size-Related Properties, and Applications toward Biology, Catalysis, and Nanotechnology. *Chem. Rev.* **2004**, *104*, 293−346.

(15) Murray, C. B.; Sun, S.; Gaschler, W.; Doyle, H.; Betley, T. A.; Kagan, C. R. Colloidal Synthesis of Nanocrystals and Nanocrystal Superlattices. *IBM J. Res. Dev.* **2001**, *45*, 47−56.

(16) Boles, M. A.; Ling, D.; Hyeon, T.; Talapin, D. V. The Surface Science of Nanocrystals. *Nat. Mater.* **2016**, *15*, 141−153.

(17) Boles, M. A.; Talapin, D. V. Many-Body Effects in Nanocrystal Superlattices: Departure from Sphere Packing Explains Stability of Binary Phases. *J. Am. Chem. Soc.* **2015**, *137*, 4494−4502.

(18) Si, K. J.; Chen, Y.; Shi, Q.; Cheng, W. Nanoparticle Superlattices: The Roles of Soft Ligands. *Adv. Sci.* **2018**, *5*, 1700179.

(19) Jishkariani, D.; Diroll, B. T.; Cargnello, M.; Klein, D. R.; Hough, L. A.; Murray, C. B.; Donnio, B. Dendron-Mediated Engineering of Interparticle Separation and Self-Assembly in Dendronized Gold Nanoparticles Superlattices. *J. Am. Chem. Soc.* **2015**, *137*, 10728−10734.

(20) Esipova, T. V.; Ye, X.; Collins, J. E.; Sakadžić, S.; Mandeville, E. T.; Murray, C. B.; Vinogradov, S. A. Dendritic Upconverting Nanoparticles Enable *In Vivo* Multiphoton Microscopy with Low-Power Continuous Wave Sources. *Proc. Natl. Acad. Sci. U. S. A.* **2012**, *109*, 20826−20831.

(21) Choi, J.-H.; Wang, H.; Oh, S. J.; Paik, T.; Sung, P.; Sung, J.; Ye, X.; Zhao, T.; Diroll, B. T.; Murray, C. B.; Kagan, C. R. Exploiting the Colloidal Nanocrystal Library to Construct Electronic Devices. *Science* **2016**, *352*, 205−208.

(22) Dong, A.; Ye, X.; Chen, J.; Kang, Y.; Gordon, T.; Kikkawa, J. M.; Murray, C. B. A Generalized Ligand-Exchange Strategy Enabling Sequential Surface Functionalization of Colloidal Nanocrystals. *J. Am. Chem. Soc.* **2011**, *133*, 998−1006.

(23) Jishkariani, D.; Lee, J. D.; Yun, H.; Paik, T.; Kikkawa, J. M.; Kagan, C. R.; Donnio, B.; Murray, C. B. Dendritic Effect and

DOI: 10.1021/acsnano.9b01107
ACS Nano 2019, 13, 5712−5719

Magnetic Permeability in Dendron Coated Nickel and Manganese Zinc Ferrite Nanoparticles. *Nanoscale* **2017**, *9*, 13922−13928.
(24) Fleutot, S.; Nealon, G. L.; Pauly, M.; Pichon, B. P.; Leuvrey, C.; Drillon, M.; Gallani, J.-L.; Guillon, D.; Donnio, B.; Begin-Colin, S. Spacing-Dependent Dipolar Interactions in Dendronized Magnetic Iron Oxide Nanoparticle 2D Arrays and Powders. *Nanoscale* **2013**, *5*, 1507−1516.
(25) Wang, D.; Deraedt, C.; Ruiz, J.; Astruc, D. Magnetic and Dendritic Catalysts. *Acc. Chem. Res.* **2015**, *48*, 1871−1880.
(26) Astruc, D.; Lu, F.; Aranzaes, J. R. Nanoparticles as Recyclable Catalysts: The Frontier between Homogeneous and Heterogeneous Catalysis. *Angew. Chem., Int. Ed.* **2005**, *44*, 7852−7872.
(27) Malassis, L.; Jishkariani, D.; Murray, C. B.; Donnio, B. Dendronization-Induced Phase-Transfer, Stabilization and Self-Assembly of Large Colloidal Au Nanoparticles. *Nanoscale* **2016**, *8*, 13192−13198.
(28) Diroll, B. T.; Jishkariani, D.; Cargnello, M.; Murray, C. B.; Donnio, B. Polycatenar Ligand Control of the Synthesis and Self-Assembly of Colloidal Nanocrystals. *J. Am. Chem. Soc.* **2016**, *138*, 10508−10515.
(29) Newkome, G. R.; Moorefield, C. N.; Vögtle, F. *Dendrimers and Dendrons*; Wiley-VCH Verlag GmbH & Co. KGaA: Weinheim, 2001.
(30) Liu, B.; Besseling, T. H.; Hermes, M.; Demirörs, A. F.; Imhof, A.; Van Blaaderen, A. Switching Plastic Crystals of Colloidal Rods with Electric Fields. *Nat. Commun.* **2014**, *5*, 3092−3099.
(31) Elbert, K. C.; Jishkariani, D.; Wu, Y.; Lee, J. D.; Donnio, B.; Murray, C. B. Design, Self-Assembly, and Switchable Wettability in Hydrophobic, Hydrophilic, and Janus Dendritic Ligand−Gold Nanoparticle Hybrid Materials. *Chem. Mater.* **2017**, *29*, 8737−8746.
(32) Dong, A.; Chen, J.; Vora, P. M.; Kikkawa, J. M.; Murray, C. B. Binary Nanocrystal Superlattice Membranes Self-Assembled at the Liquid-Air Interface. *Nature* **2010**, *466*, 474−477.
(33) Wang, D.; Hermes, M.; Kotni, R.; Wu, Y.; Tasios, N.; Liu, Y.; de Nijs, B.; van der Wee, E. B.; Murray, C. B.; Dijkstra, M.; van Blaaderen, A. Interplay between Spherical Confinement and Particle Shape on the Self-Assembly of Rounded Cubes. *Nat. Commun.* **2018**, *9*, 2228.
(34) Jishkariani, D.; Wu, Y.; Wang, D.; Liu, Y.; van Blaaderen, A.; Murray, C. B. Preparation and Self-Assembly of Dendronized Janus Fe 3 O 4 − Pt and Fe 3 O 4 − Au Heterodimers. *ACS Nano* **2017**, *11*, 7958−7966.
(35) Diroll, B. T.; Weigandt, K. M.; Jishkariani, D.; Cargnello, M.; Murphy, R. J.; Hough, L. A.; Murray, C. B.; Donnio, B. Quantifying "Softness" of Organic Coatings on Gold Nanoparticles Using Correlated Small-Angle X-Ray and Neutron Scattering. *Nano Lett.* **2015**, *15*, 8008−8012.
(36) Zanchet, D.; Moreno, M. S.; Ugarte, D. Anomalous Packing in Thin Nanoparticle Supercrystals. *Phys. Rev. Lett.* **1999**, *82*, 5277−5280.
(37) Fortini, A.; Dijkstra, M. Phase Behaviour of Hard Spheres Confined between Parallel Hard Plates: Manipulation of Colloidal Crystal Structures by Confinement. *J. Phys.: Condens. Matter* **2006**, *18*, L371−L378.
(38) Hodges, J. M.; Morse, J. R.; Williams, M. E.; Schaak, R. E. Microscopic Investigation of Chemoselectivity in Ag-Pt-Fe_3O_4 Heterotrimer Formation: Mechanistic Insights and Implications for Controlling High-Order Hybrid Nanoparticle Morphology. *J. Am. Chem. Soc.* **2015**, *137*, 15493−15500.

DOI: 10.1021/acsnano.9b01107
ACS Nano 2019, 13, 5712−5719